ELSEVIER

Contents lists available at ScienceDirect

#### Biosensors and Bioelectronics

journal homepage: www.elsevier.com/locate/bios



# Revealing cell-substrate adhesion at subcellular resolution with ultra-flat field-effect transistor arrays

Ziyu Gao <sup>a</sup> , Susanne Schäfer <sup>b</sup>, Regina Stockmann <sup>b</sup>, Bernd Hoffmann <sup>c</sup>, Rudolf Merkel <sup>c</sup>, Andreas Offenhäusser <sup>b</sup> , Sven Ingebrandt <sup>a,\*</sup>

- <sup>a</sup> Institute of Materials in Electrical Engineering 1, RWTH Aachen University, Aachen, 52074, Germany
- b Institute of Biological Information Processing, Bioelectronics (IBI-3), Forschungszentrum Jülich GmbH, Jülich, 52428, Germany
- <sup>c</sup> Institute of Biological Information Processing, Mechanobiology (IBI-2), Forschungszentrum Jülich GmbH, Jülich, 52428, Germany

#### ARTICLE INFO

# Keywords: Electric cell-substrate impedance sensing (ECIS) Impedance spectroscopy Field-effect transistors cell-substrate impedance sensing (FETCIS) Transistor-transfer function (TTF) Cell-transistor interaction Single cell dynamics Membrane attachment

#### ABSTRACT

In vitro models with isolated cells play an essential role in biological studies, acting as a bridge between complex in vivo research and acellular biomolecular studies. Moving beyond conventional cell-based research methods, which typically require fluorescence labeling of specific biological cues, Electric Cell-substrate Impedance Sensing (ECIS) enables the monitoring of cell adhesion, proliferation, and migration without the need for labels. This work goes beyond the classical ECIS technique utilizing ultra-flat field-effect transistors (UF-FETs) for cell-substrate adhesion experiments at single-cell and even sub-cellular level. Planar surfaces of UF-FETs were achieved by local oxidation of silicon. We monitored the adhesion of cells to the open gates of the UF-FETs using the transistor-transfer function method. This enables non-invasive, real-time monitoring of cells, including cell adhesion, migration and apoptosis- and necrosis-like behavior. To demonstrate single cell resolution, we used fibroblasts from the umbilical cord of rats and induced them to migrate. With our technique we were also able to detect the movement of small lipid vesicles at the gates of UF-FETs demonstrating their ability to monitor the dynamics of soft and fluidic artificial membranes in real-time. Finally, we validated the label-free concept with a less complex and smaller cell model - erythrocyte ghost cells. Our experiments demonstrate that UF-FETs can be used in single-cell tracking and advanced studies for real-time monitoring of artificial membranes on solid surfaces, bridging the gap between biological evaluation and bioelectronic readout.

#### 1. Introduction

Over the past decades, Electric Cell-Substrate Impedance Sensing (ECIS) established a solid foundation for monitoring cell cultures in a label-free and non-invasive manner (Giaever and Keese, 1984, 1991, 1993). ECIS has been extensively used in various bioassays (Shoute et al., 2023; Stolwijk and Wegener, 2019; Vora et al., 2023). However, single cell studies with this technique are difficult, since for reliable recordings, the minimum sizes of the recording microelectrodes vary from 25  $\mu m$  to 250  $\mu m$  in diameter. Therefore, many cellular assays in ECIS are done with cell lines forming dense layers. In this case, ECIS is even capable to record changes in cell-cell junctions, membrane capacitance and sealing resistance of the cell-substrate contact. The limitation of ECIS in terms of lateral dimensions have been explored (Pradhan et al., 2012; Susloparova et al., 2015) and different approaches

to optimize electrode designs were described (Price et al., 2009; Rahman et al., 2007). It was concluded that the lower size limit for metal electrodes for reliable bioimpedance assays of cell cultures is 50 µm in diameter (Rahman et al., 2007). In this respect, field-effect transistors (FETs) have shown great potential to advance the lateral detection limits to the single-cell level (Hempel et al., 2015; Schäfer et al., 2009; Susloparova et al. 2013, 2015). Beyond cell-chip interactions, FETs have also demonstrated their capabilities in DNA detection (Ingebrandt et al., 2007; Uslu et al., 2004), protein detection (GhoshMoulick et al., 2009), biomarker detection (Schoning and Poghossian, 2002) and as immunosensors (de Moraes and Kubota, 2016) through specific surface functionalization.

To enhance sensitivity in cellular monitoring and analysis while downsizing bioelectronic chips, the transistor-transfer function (TTF) readout method was developed and applied with micro-scale resolution

This article is part of a special issue entitled: Biosensors 2025 published in Biosensors and Bioelectronics.

E-mail address: ingebrandt@iwe1.rwth-aachen.de (S. Ingebrandt).

<sup>\*</sup> Corresponding author.

in our previous research (Hempel et al., 2019; Ingebrandt et al., 2007; Schäfer et al., 2009; Koppenhöfer et al., 2013; Susloparova et al., 2015). By applying a sinusoidal signal with a specific voltage amplitude and varying frequency from 1 Hz to 1 MHz via the reference electrode, which is also used to apply the DC bias voltage to the electrolyte gate, changes in bandwidth caused by biological sample interactions with the gate oxide of the FETs were identified (GhoshMoulick et al., 2009; Ingebrandt et al., 2007). This novel approach demonstrated the detection of cell-substrate adhesion at the single-cell level in real-time, highlighting the capability to further study cell-chip interfacing dynamics.

One of the main challenges to move the TTF technology forward arises from the highly customized transistor designs, where cell-chip interactions lack standardization. Chip topography and surface roughness have emerged as critical factors for biointerfacing, as they can trigger mechanosensitive responses and result in topography-specific features in the cytoskeleton (Hou et al., 2020). Changes in cell functions may also occur due to alterations in the mechano-biological environment (Abagnale et al., 2015; Blaschke et al., 2020). As a result, sensing intermediate cellular changes such as adhesion, detachment, and migration - closely related to membrane stiffness, viscoelasticity, and fluidity - becomes possible (Humphrey et al., 2014; Hurst et al., 2021). Planar substrates have been commonly used as standard surfaces in common in vitro models to minimize the topographical influence on cell interfacing (Solowiej-Wedderburn and Dunlop, 2022). To further advance specific cell mechanistic recognition with biosensors, efforts have been made to flatten the transistor surface to achieve a seamless cell-chip contact, providing a direct bio-signaling path between the cell membrane and the transistor chips (Koppenhöfer et al., 2015b; Susloparova et al., 2014).

To understand the recorded TTF spectra, a reliable electrical and analytical model is required to quantitatively decipher the complex biological environment (Leung et al., 2022), where numerous factors are involved in cell adhesion, apoptosis and migration processes (Hurst et al., 2021). In 2015 we published an analytical model to describe the cell-transistor adhesion on a single cell level and to differentiate between cellular detachment and morphological changes. Other, advanced optical technologies to quantify real-time membrane-substrate interactions have also been described (Braun and Fromherz, 2004; Fromherz et al., 1999; Zeck and Fromherz, 2003). Lipid membranes, widely used as artificial cell membranes, are promising candidates to investigate membrane-chip interactions as a bottom-up model (Atanasov et al., 2005). For example, the association rate of ligand proteins incorporated into lipid membranes could potentially be utilized to understand protein complexation and cell recognition (Bihr et al., 2014). Understanding membrane-chip interaction appears to be a promising approach to unveil cell-chip interfacing dynamics.

This work reports our progress in fabricating and utilizing ultra-flat field-effect transistors (UF-FETs) to reveal cell-substrate adhesion mechanics with so far unreachable resolution. We demonstrate real-time and non-invasive single-cell monitoring, including cell adhesion, necrosis, apoptosis, and migration on a single-cell and even sub-cellular level. In the presented assays, however, proof-of-concept experiments are provided, since the number of transistors per chips was very low (16 transistors channels in a 4x4 array). This limited number did not permit dose-response dependent biological assays with the analyzed cells.

To expand the possibilities of biomaterial-transistor interfacing experimentally, another biophysical interface model is demonstrated by attaching lipid membrane vesicles to the UF-FETs. Even the attachment of lipid vesicles was observed with significant sensitivity, providing valuable insights into the real-time monitoring of the dynamics of soft and fluidic artificial membranes. The concept was further validated using a simpler and more natural membrane vesicle model - erythrocyte ghost cells (anucleated cells). By providing solid evidence of the use of UF-FETs for single-cell tracking and advanced functions for artificial membrane monitoring in real-time, this work highlights its potential in bridging the gap between biological evaluation and biophysical

fundamentals, offering novel perspectives on understanding both native and artificial membrane-chip interactions.

#### 2. Materials and methods

#### 2.1. FET chip design

FETs were fabricated according to our previously optimized design parameters (Offenhausser et al., 1997; Schäfer et al., 2009; Susloparova et al. 2013, 2014; Uslu et al., 2004) with respect to transistor pitches, dimensions of contact lines (drains and common source), bond pads and chip sizes. To realize very robust devices, we used implanted contact lines in the silicon chip, since in contrast to metal tracks these can be very reliably passivated by oxidation processes. Sixteen transistors in a  $4 \times 4$  array with a distance of 200  $\mu m$  were placed in the middle of  $5 \times 5$ mm<sup>2</sup> chips, as illustrated in Fig. S1. In the design of this study, we optimized the areas of all contact lines such, that each transistor has the same contact line resistance and capacitance. This is very important when the 16-channel devices are utilized in TTF readout mode, since the contact line parasitic parameters primarily define the low pass characteristics of the recorded spectra. Different gate geometries with 3, 4 or 5 um in length and 6, 12 or 25 um in width, respectively, were processed. These microscale sizes enable single cell studies, since the sensitive gate areas are significantly smaller than the typical diameters of ECIS electrodes as discussed above.

#### 2.2. FET chip fabrication

The planar FET chips were fabricated in a process flow similar as previously reported (Offenhausser et al., 1997; Schäfer et al., 2009; Susloparova et al. 2013, 2014; Uslu et al., 2004). We added specific fabrication steps to achieve almost perfectly flat surfaces. In our former processes, the implantation and contact line passivation process steps with grown silicon oxide and deposited silicon nitride usually resulted in a significant topography of the open-gate areas of several hundred nanometers. In an earlier work, we described a simpler method to achieve almost flat chip surfaces for the contact line regions, but not for the gate regions, which had a remaining topography of 220 nm (Koppenhöfer et al., 2015b). In this former process, we omitted the contact line passivation almost completely with the drawback of very high contact line parasitic values. In this earlier work we already showed that the migration of cells over the contact line edges was unhindered compared to cell cultures on FET arrays having a topography. However, in this much simpler fabrication process, the gate areas, as the sensitive regions of the FETs, had a remaining topography and the bandwidth of the devices was strongly limited. The fabrication challenge to realize a completely flat topography is that the contact lines, typically tracks of implanted silicon, need to be passivated at best with a sandwich layer of silicon oxide-silicon nitride-silicon oxide (ONO-stack), while the gate areas use only a very thin silicon oxide layer (10 nm) typically grown in a dry oxidation process at 820 °C to achieve a high-quality gate oxide with a low density of interface states for low noise transistors. Usually, at later stages in the process, the ONO passivation layer is opened and the gate oxide is grown.

In this work, to achieve almost perfectly planar open-gate UF-FET arrays, local oxidation of silicon (LOCOS) and precise end-point etching of silicon oxide to the contact line levels were utilized. In LOCOS processes it is well known that the silicon oxide growth rate underneath a dense silicon nitride layer is significantly diminished. In the fabrication process in this work, 100 mm silicon wafers with low n-type doping were used as substrates. Firstly, 30 nm of dry silicon oxide were thermally grown and 100 nm of silicon nitride were deposited by low pressure chemical vapor deposition (LPCVD). The drain and source regions were defined by structuring the nitride and oxide layers by a first lithography. The contact line regions were doped by a double implantation of boron ions (Boron 120 keV at 8•10<sup>15</sup> 1/cm<sup>2</sup> dose and 80 keV at 5•10<sup>15</sup> 1/cm<sup>2</sup>

dose) to create a combination of Gaussian shaped profiles beneath the wafer surface (Sze, 2012). The gate plateau area was defined by a second lithography. A layer of dry silicon oxide was grown as a protection layer by LOCOS of silicon oxide after a standard RCA (Radio Corporation of America) cleaning procedure. The planarization was realized by selective silicon oxide etching with hydrofluoric acid (HF 1 %) to the same height as the nitride layer on the protected gate areas by precise timing. Afterwards a selective wet etching step with boiling phosphoric acid (H $_3$ PO $_4$  at 155  $^\circ$ C) was applied for the silicon nitride gate protection leading to the same height and ensuring ultra-flat gate areas. This was ensured by several test wafers and by using atomic force microscopy (AFM) characterization.

The third lithography was applied to define the drain, source, and the position of the gate areas. A second boron implantation was used (80 keV at  $5 \cdot 10^{15} \ 1/\text{cm}^2$  dose) to contact the feed line to the source and drain contact areas and to define the gate length. Following a reactive ion etching process (O<sub>2</sub>) to remove the resist and another RCA cleaning step, the wafers were annealed at 900 °C and the grown silicon oxide (~13 nm) was etched away with HF 1 %. Subsequently, dry oxidation of the gate oxide was applied at 820 °C.

A fourth lithography was used to define the metal contact windows between the implanted source and drain regions by opening the silicon oxide passivation. Metal feedlines were defined by a fifth lithography in an image reversal process. The metal leads were structured by a triplelayer metal deposition (150 nm Aluminum/10 nm Titanium/150 nm Gold) followed by a lift-off step. Compared to our previous designs, the metal contact lines were longer for the outer FETs inside the array (Fig. S1) to achieve the same contact line parasitic values (capacitance and resistance) for all channels. The wafers were thermally annealed at 325 °C to ensure Ohmic contacts between the metal and the implanted silicon contact lines. Finally, the wafers were diced into single chips using a resist protection layer. Chips for further measurements were assembled by integration into dual in line sockets and wire bonding (Offenhausser et al., 1997; Schäfer et al., 2009; Uslu et al., 2004) or by the flip-chip method (Koppenhöfer et al., 2015a; Miller, 2000) as previously described. To enable cell cultures on the chip surfaces, a glass ring and usage of polydimethylsiloxane (PDMS) (Sylgard 96-083, Dow Corning, Germany) formed small petri-dish like culture chambers, respectively.

#### 2.3. Transistor-transfer characteristics of the UF-FET chips

Typically, the response of ion-sensitive field-effect transistors (ISFETs) is recorded by monitoring the change in drain-source current, which is caused by a change of the effective potential applied at the gate oxide. This readout mode is the classical potentiometric method, where the change in drain-source current can be described by an effective change of the potential at the gate. It is well-known that in this potentiometric readout mode one can utilize ISFETs for the detection of pH changes in the solution, for the detection of charged molecules such as DNA or in enzymatic bioassays, where a biomolecular conversion of an analyte leads to changes in the pH value. In contrast to this, impedance spectroscopy of ISFETs can be used to monitor changes at the transistor gate causing a difference in the device's input impedance. For this purpose, the FET devices need to be operated at a constant working point. To find this working point, the transfer characteristics of UF-FETs were measured before and after encapsulation with two different setups. Before encapsulation, the output  $I_{DS}$  ( $V_{DS}$ ) and transfer  $I_{DS}$  ( $V_{GS}$ ) characteristics of chips were measured with a wafer probe station. The transconductance values (gm) were calculated by the numerical derivation of IDS (VGS).

After encapsulation, the chips were characterized with a 16-channel TTF amplifier system (Han et al., 2006; Ingebrandt et al., 2007; Law et al., 2015; Schäfer et al., 2009) as shown in Fig. S2, which was developed by our team and built in house. As earlier described, this amplifier system can record all 16 transistor channels in parallel in

either dc- or ac-readout mode. For the impedimetric ac-readout mode, it uses 16 individual channels of phase-selective amplification, which records the real part of the transistor-transfer function. To contact the open-gate transistors, the chips were filled with electrolyte solution (extracellular patch-clamp solution: NaCl (140 mM), KCl (5 mM), glucose (5 mM) and HEPES (10 mM) in double distilled  $\rm H_2O$  (pH 7.4)), which was contacted with an Ag/AgCl electrode. The usage of such defined electrolyte solutions ensured the reproducibility of all cell-based assays. All 16 transistors in each chip were initially characterized and their transconductance values  $\rm g_m$  were calculated. This procedure was repeated each time before cell measurements and the transistors were set to a working point with a high transconductance value. For impedimetric readout, the individual TTF spectra for each channel were taken by sweeping a small sinusoidal stimulation voltage of 20 mV over a frequency range from 1 Hz to 1 MHz.

#### 2.4. Cell culture and maintenance

Human embryonic kidney (HEK) 293 cells were chosen in this work for cell adhesion, detachment, apoptosis and necrosis measurements due to their low endogenous ionic current densities (Zhu et al., 1998) and their strong adhesion with minimum distance from the oxide surfaces (Sommerhage et al., 2008; Wrobel et al., 2008). M10 all culture medium supplemented with glutamine (2 mM), non-essential amino acids (1 % v/v), fetal calf serum (FCS, 10 % v/v), penicillin (100 units/mL) and streptomycin (0.1 ng/mL) were used for cell maintenance (all VWR International GmbH, Germany). Cells were cultured in 50 mm petri dishes and split at around 70 % confluence by trypsin. Cultures were maintained in a 5 % CO $_2$  incubator at 37 °C until usage in experiments.

Fibroblasts cells were taken from rat umbilical cords harvested from Sprague-Dawley rat embryos (Charles River, Sulzbach, Germany) at embryonic day 15–18. Fibroblasts were chosen for cellular migration studies due to their sensitive motility and their role as a preferred model in migration research. Endothelial cell growth medium containing basic fibroblast growth factor (human, recombinant, 1.0 ng/mL medium), endothelial cell growth supplement/Heparin (4  $\mu$ L/mL medium), epidermal growth factor (human, recombinant, 1.0 ng/mL medium), hydrocortisone (1  $\mu$ g/mL medium), phenol red (0.62 ng/mL medium) and FCS (20  $\mu$ L/mL medium) were used for the fibroblast culture (all VWR International GmbH, Germany). Cells were maintained in a 5 % CO<sub>2</sub> incubator at 37 °C until usage in experiments.

#### 2.5. HEK 293 cell adhesion and detachment monitoring with UF-FETs

For the HEK 293 cell adhesion measurements using the UF-FETs,  $1.5-2.5 \times 10^3$  HEK 293 cells (in 25  $\mu$ L M10 medium) were plated onto the encapsulated transistor chips, reaching a final density between 240 and 410 cells/mm<sup>2</sup> on the open chip area for cell cultures (funnel diameter 2.8 mm). Chips were filled with 475 µL M10 medium after 3-h settling time. Cells were cultured for 2-3 days to reach a total cell density of around  $8 \times 10^3$ /chip. Before the measurements, the culture medium was replaced with calcium-free extracellular patch-clamp solution at 37  $^{\circ}\text{C}$  to ensure reproducible conditions for all experiments. For the cell adhesion measurements, the chips were mounted to the TTFamplifier system and its temperature control was set to 37 °C. The transistors were biased by applying respective drain-source and gatesource voltages (typically  $V_{DS} = -2.5 \; V, \, V_{GS} = -2 \; V$ ) to their working points of highest transconductance values. An alternating voltage of 20 mV was applied to the reference electrode forming the electrolyte gate contact. To correlate changes in the spectra with cell attachment or detachment, the position of the cells on the transistor area was checked by an upright light microscope (Zeiss Axiotech Vario with a 10× longdistance objective, differential interference contrast microscopy, Carl Zeiss Microscopy GmbH, Germany) in parallel. Unfortunately, we had no chance to align the cells onto the transistors to increase the yield of our experiments as described for neuronal cells in some of our earlier experiments (Lauer et al., 2001). Cells were seeded, the adhesion situation was optically checked and cell-adherent transistors were analyzed. In the cell adhesion measurements, the TTF spectra were measured first with cells and then without cells after mechanically removing the adherent cells from the chip with a Q-tip soaked with ethanol.

To monitor the cell detachment in a time-dependent mode, a first transfer-function characterization was done to determine the significant frequency range. Then, time-dependent measurements were applied at a constant frequency, where the largest differences were expected (typically 100–200 kHz). Trypsin (VWR International GmbH, Germany) was used to induce the cell detachment without mechanical force. 200  $\mu L$  trypsin was applied to each chip and the detachment of the cells from the gate was monitored both electronically and optically. After the complete cellular detachment, a frequency-dependent measurement was repeated with all gates to enable a fit of the recorded TTF spectra to the equivalent electrical circuit model.

#### 2.6. HEK 293 cell necrosis and apoptosis monitoring with UF-FETs

To simulate a cell necrosis assay as a proof-of-concept, the ionophore Amphotericin B (AmB, PAN-Biotech GmbH, Germany) was chosen to bind sterins at the cell membrane and to permeabilize it for potassium ions (K $^+$ ). This artificial process induces similar effects like a natural necrosis process, while with higher concentrations a signaling pathway leading to nephrotoxicity is triggered (Cheng et al., 1982; França et al., 2014; Varlam et al., 2001). 200  $\mu L$  AmB (0.1 mg/mL) were applied to each chip to induce this artificial necrosis process, which is a concentration clearly above the critical concentration to favor necrotic over apoptotic pathways (Varlam et al., 2001). Same frequency- and time-dependent measurement were applied with the TTF-amplifier system as already stated above, together with optical monitoring.

To monitor the apoptosis dynamics, the anti-cancer agent irinotecan hydrocholoride (CPT-11) was used to permeabilize the cell membranes (Wall et al., 1966). This was previously described to trigger a natural apoptosis process in HEK 293 cultures (Conti et al., 1996; Wu et al., 2016). 200  $\mu L$  CPT-11 containing solution (with the apoptosis markers annexin-V and propidium iodide (all VWR International GmbH, Germany)) was applied to each chip, following with 60–110 min incubation. Both frequency- and time-dependent measurements were done with the TTF-amplifier system as stated above, together with parallel fluorescence microscopy using the upright Zeiss microscope. Electrical measurements were continued while the UV-light was off during the incubation period. After apoptosis induction, transfer-function measurements were repeated.

#### 2.7. Fibroblast migration on UF-FETs

For the migration measurements,  $2-15 \times 10^3$ /chip fibroblast cells were plated onto the fibronectin-coated UF-FET chips and maintained in culture for 1-2 days in a 5 % CO2 incubator at 37 °C. To stimulate cell migration, 50 nM epidermal growth factor (EGF) was added 1 h before the measurements. Then the chips were mounted to the TTF-amplifier system and maintained at 37 °C. Fibroblast cell culture medium was directly used as the electrolyte in these experiments, which was contacted by a Ag/AgCl wire as the electrolyte-gate contact. The transistors were set to their working point and TTF measurements were done as described above. The position of the cells on the transistor area was checked optically with a high-resolution upright microscope to distinguish gates with adherent cells from cell-free transistor gates, and the TTF spectra were measured before starting the time-dependent measurements. These time-dependent measurements were then done by applying a constant frequency of the stimulation voltage (100 kHz), while monitoring the signal amplitude. In parallel, a time series of images were taken with one photo per minute to correlate cell motion and electrical adhesion signal. In the supplementary material a video can be seen, which was generated out of these microscopy images.

#### 2.8. Lipid vesicle preparation and vesicle-UF-FET interaction monitoring

Lipid vesicles were prepared by the liposome electroformation method (Angelova and Dimitrov, 1986; Dimitrov and Angelova, 1988). We prepared vesicles by the electroswelling technique from planar electrode surfaces (Angelova and Dimitrov, 1987; Estes and Mayer, 2005). Lipids from Avanti Polar Lipids Inc., 1-Stearoyl-2-Oleoyl-sn-Glycero-3-Phosphocholine (SOPC), 1-Stearoyl-2-Oleoyl-sn-Glycero-3-[Phospho-L-Serine] (SOPS) and 1,2-Dimyristoyl-sn-Glycero-3-Phosphoethanolamine-N-LissamineRhodamine-B-Sylfonyl (DMPE-LisRhod) were used. 2  $\mu L$  of lipid mixture (SOPC:SOPS:DMPE-LisRhod = 500:2:1) were carefully deposited on indium tin oxide (ITO) coated glass. The lipid-chloroform film was dried under vacuum for 1 h. After dehydration, the glasses were arranged in a chamber containing 2 mL sucrose solution (300 mM). The glasses were separated with a 1 mm Teflon spacer and connected to copper electrodes. For electroswelling, an AC field (2 V) was applied at 10 Hz for 3 h. Driven by osmotic and electrostatic forces, the lipid molecules formed liposomes. After preparation, we transferred these lipid vesicles carefully into a glucose buffer (300 mM) supplemented with PBS (pH 7.4) and measurements were done within a few hours. For TTF-measurements, the surfaces of the UF-FETs were coated with positively charged poly-L-lysine (PLL, MW: 150-300 Da, Sigma-Aldrich, Germany) to ensure an electrostatic interaction with the negatively charged lipid vesicles. Osmolarities of the intra- and extra-vesicular solutions were set to 300 mOsm and 310 mOsm, respectively, to allow membrane elasticity and to ensure that the vesicles adapt to the UF-FET surfaces smoothly.

For the TTF measurements, UF-FET chips were firstly characterized with glucose solution as a measurement electrolyte, and frequency-dependent measurements were taken as reference. Then vesicles were carefully added by a bovine serum albumin (BSA, Sigma-Aldrich, Germany) coated pipette to avoid vesicle membrane rupture. After 30 min settling time, the chip surfaces were photographed and a second frequency-dependent measurement was performed.

### 2.9. Erythrocyte ghosts' preparation and erythrocyte-UF-FET interaction monitoring

Erythrocyte ghosts were prepared by direct hypotonic lysis of red blood cells (Lisin et al., 1996; Steck and Kant, 1974). Briefly, the erythrocyte-membrane was collected by ultracentrifugation in a lysis buffer and subsequently transferred to an isotonic buffer, which leads to the resealing of the membrane and is resulting in the resealed ghosts.

For the preparation, 25 mL of fresh human blood was used, supplemented with heparin (Sigma-Aldrich, Germany) to prevent coagulation. A first centrifugation step (4 °C, 2300×g, 10 min) was applied to separate the blood serum from all cellular components. The pellet was collected and dissolved in PBS buffer (12 mL, pH 8.0) for the next centrifugation (repeated three times until the supernatant was clear). The pellet was then dissolved in ice-cold hypotonic buffer (5P8, Na<sub>3</sub>PO<sub>4</sub>, 5 mM, pH 8.0) to initiate hemolysis of the cells. The erythrocyte ghosts were transferred to sterile ultracentrifuge tubes and pelleted at 4 °C, 22000×g for 15 min, following with two times washing in ice-cold 5p8-Mg solution (5P8 with MgSO<sub>4</sub>, 1 mM, pH 8.0) at 4  $^{\circ}$ C, 22000 $\times$ g for 15 min to induce immediate sealing. The sealed ghosts were washed twice in ISP solution (5P8 supplemented with sucrose: 9g per 100g 5P8, pH 7.4) and re-suspended in 4 mL of the same solution. Antibiotic was added (1.5 µL/mL solution (G-418, Sigma-Aldrich, Germany)) and the ghost density was controlled optically. The erythrocyte ghost solution was stored at 4 °C until measurements.

For TTF-measurements, the erythrocyte ghosts were plated on the UF-FET chips and stored at 4  $^{\circ}$ C while sinking to the surface. After 30–45 min, TTF-measurements were conducted at room temperature. The ISP buffer was used as the electrolyte solution in this case. Optical monitoring of erythrocyte ghost-UF-FET chip interaction was carefully carried out with a water immersion objective (UMPlanFl 20× Water Immersion Microscope Objective, Olympus Europa SE & Co. KG,

Germany) to avoid erythrocyte ghost detachment caused by shear forces.

#### 2.10. Modeling the TTF spectra

To understand and explain the UF-FET TTF spectra in this work, additional factors including reference electrode impedance, buffer solution resistance, FET parasitic parameters and the transfer characteristics of the amplifier stage need to be taken into account. When including the influences of all these side-parameters into a model, the cell-related parameters such as seal resistance to the surface and the projected cell membrane capacitance can be extracted. We earlier presented an electrically equivalent circuit model (EEC) to describe the complete experimental configuration (Hempel et al., 2015; Morgan et al., 2007; Schäfer et al., 2009; Susloparova et al., 2015).

For a precise cell-transistor contact model, the cellular membrane needs to be divided into free membrane area and membrane area attached to the surface. The electrolyte-filled cleft between the attached part of the cellular membrane and the transistor gate surface forms a resistive path in form of a planar plate resistor ( $R_{\rm seal}$ ). For a first approximation in single cell experiments, the part of the EEC related to cell-related parameters can be simplified into only two major elements the projected membrane area  $C_{PM}$  and the total resistance of the membrane  $R_{\rm mem}$ . Together with the sealing resistance  $R_{\rm seal}$ , which describes the adhesion strength, these parameters are related to cell morphology and membrane integrity, respectively. As described before, this model enables to extract the adhesion strength of cells to the transistor gates and even reveals the morphology of the cell on top of the transistor (Susloparova et al., 2015).

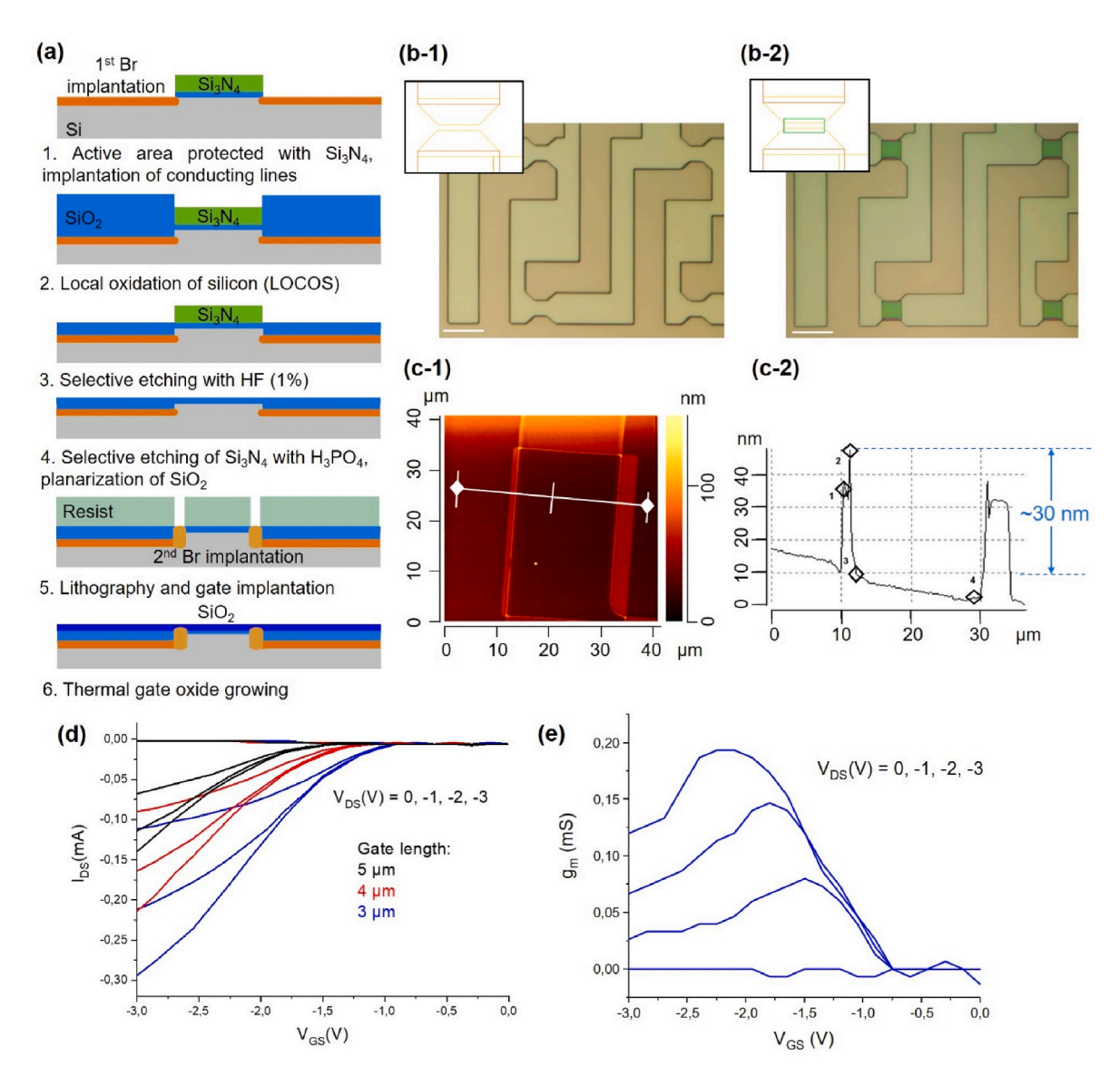


Fig. 1. Design, fabrication and characterization of UF-FETS chips: (a) Fabrication process flow of UF-FETS. We used implanted contact lines to realize robust chips for repeated usage in cell cultures. Two implantations were done to define contact lines and transistor gates. Ultra-flat surfaces were realized by the use of LOCOS oxidation and a series of wet etching of silicon oxide and silicon nitride. (b) Selected presentation of FETs design and optical image illustration during processing: (b-1) conducting lines definition by 1st lithography and gate plateau definition by 2nd lithography. Scale bar:  $50 \mu m$ . (c) Morphological characterization of gate opening after planarization by AFM. (c-1) AFM image of a gate surface, (c-2) quantification of the gate profile showing only  $\sim$ 30 nm feature heights. (d) Transfer characteristics of exemplary UF-FETs with various gate geometries or 6x5, 6x4 and 6  $\times$  3  $\mu m$  (width x length), (e) transconductance calculated by derivation of  $I_{DS}$  ( $V_{GS}$ ) for the 6  $\times$  4  $\mu m$  transistor. In this case, a working point of  $V_{DS} = -3V$  and  $V_{GS} = -2.2V$  would be selected for TTF measurements.

#### 3. Results and discussion

#### 3.1. Ultra-flat FET chip fabrication and characterization

The UF-FET fabrication process was successfully conducted as illustrated in Fig. 1a. In this process, transistors with a gate length of 3, 4 or 5  $\mu m$ , and varying gate widths of 6  $\mu m$ , 12  $\mu m$  and 25  $\mu m$  were successfully fabricated (Fig. 1b). It should be noted that the electronically effective

gate lengths are determined by under-diffusion of dopants in the gate area and can be estimated between 1 and 3  $\mu m$ , respectively. Moderate gate lengths were chosen and gate dimensions were optimized to guarantee sufficiently high  $g_m$  values for successful cell adhesion detection, while enabling experiments on the single cell level.

The surface topography of silicon nitride and oxide layers was minimized by HF and H<sub>3</sub>PO<sub>4</sub> wet etching. The etching times were balanced according to the thickness of the silicon oxide and silicon

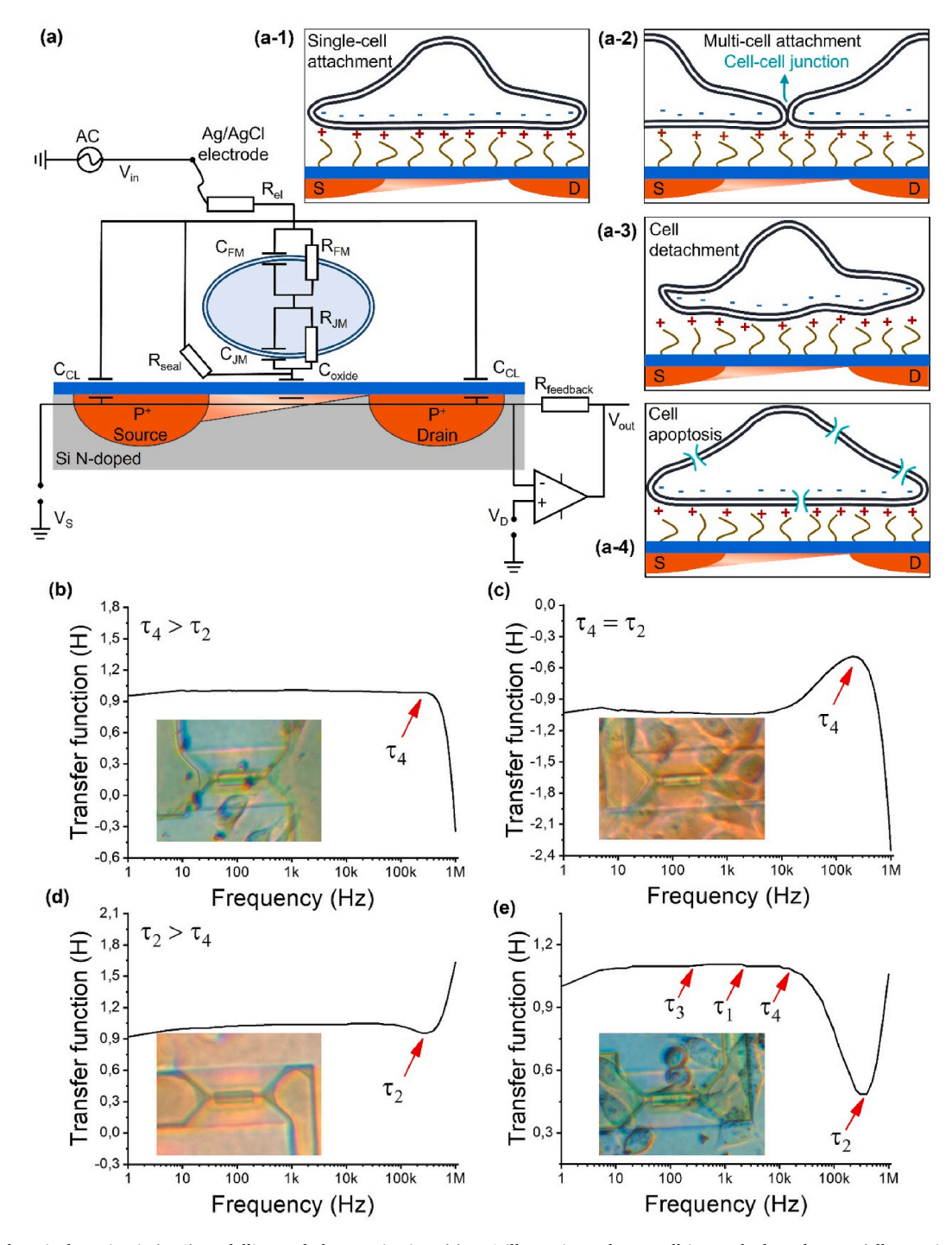


Fig. 2. Electrical equivalent circuit (EEC) modelling and characterization: (a) EEC illustration, when a cell is attached on the FET (all gate sizes  $4 \times 12 \ \mu m^2$ ) in various cell dynamic conditions such as: single cell attachment (a-1), multi-cell attachment (a-2), cell detachment (a-3) and cell apoptosis (a-4). (b–e) Influence of the time constants on the TTF spectra, characterized and analyzed with cell-free gates when  $\tau_4 > \tau_2$  (b),  $\tau_4 = \tau_2$  (c), and  $\tau_2 > \tau_4$  (d). Four different time constants are visible, when a cell is strongly attached to the transistor gates (e). HEK 293 cells were used to evaluate the transfer-function spectra. Displayed results represent typical recordings. Experiments were done with multiple chips (>10 devices) in multiple biological repeats (>3). All measurements were taken with parallel optical control as shown in the microscopy images inside the insets.

nitride layers. A series of silicon oxide and silicon nitride wet etching achieved quasi planar surfaces. After optimization and repeated controls via AFM measurements, planar surfaces in the gate areas of the UF-FET devices with step heights below 30 nm were achieved (Fig. 1c).

All transistors demonstrated typical electronic characteristics with

distinct threshold voltages in the range of -1.1 to -1.9 V and moderate subthreshold slopes between 100 and 130 mV/dec. In our process, the threshold voltages of the FETs are predominately determined by the annealing process after the second implantation, the gate dimensions and the thickness of the gate oxide. As the most important parameter,

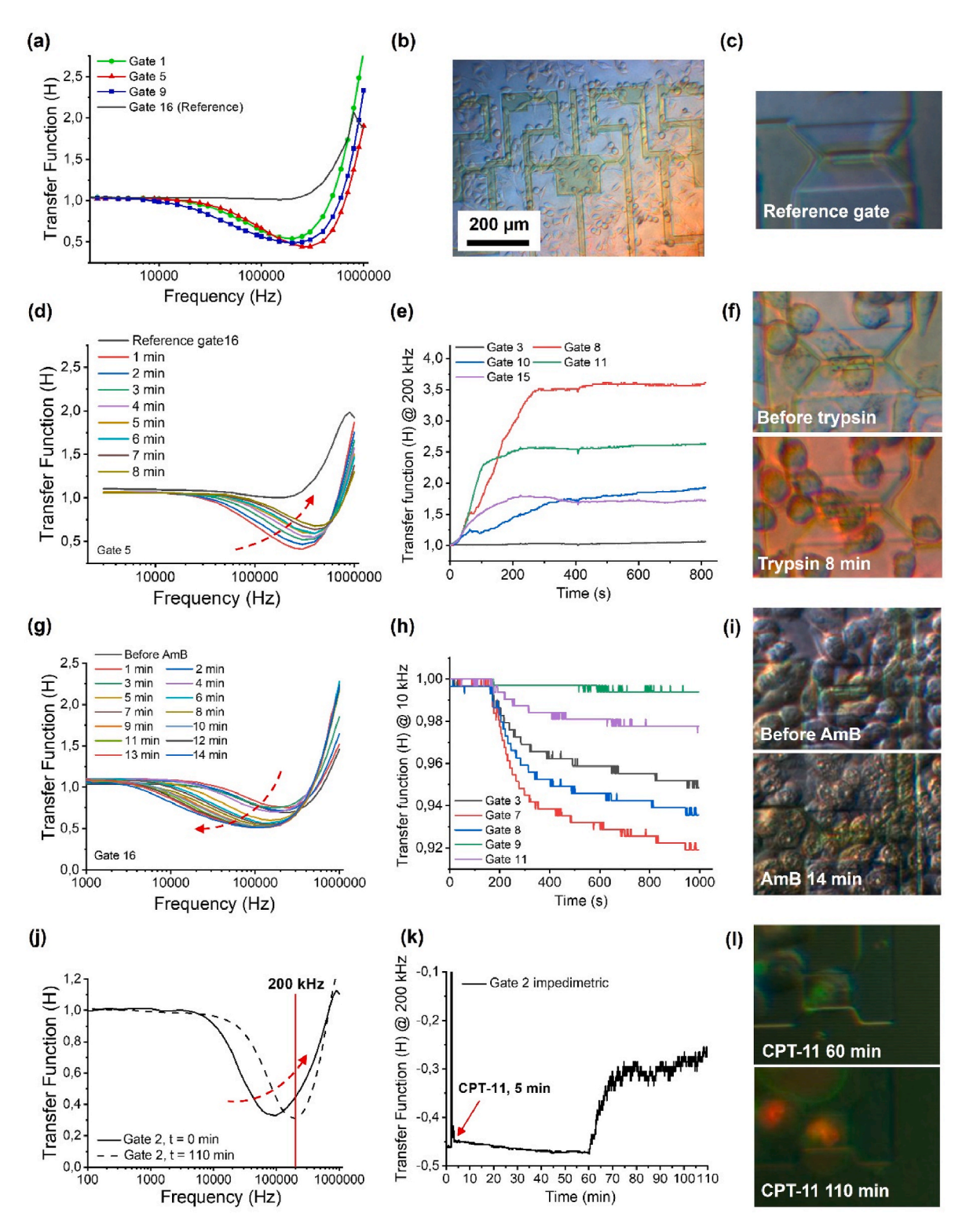


Fig. 3. Dynamic monitoring of adherent cells (HEK 293) by the transistor-transfer function utilizing the UF-FETs developed in this work. Cell adhesion can be monitored with the 16-channel ISFET array on individual cells revealing their adhesion status (a–c), Cell detachment triggered by trypsin (gate sizes  $4 \times 12 \mu m^2$ ) (d–f), cell necrosis triggered by AmB (gate sizes  $5 \times 12 \mu m^2$ ) (g–i) and cell apoptosis triggered by CPT-11 (gate sizes  $4 \times 12 \mu m^2$ ) (j–k). Both frequency-dependent (d, g, j) and time-dependent (e, h, k) measurements were applied, together with optical controls (f, I, l). The microscope is equipped with red and green fluorescence and changes in apoptosis state can be monitored (l).

the maximum transconductances  $g_m$  of the fabricated FETs were extracted (presented in Fig. 1d–e, Fig. S3 and Table S1). In Fig. 1d some exemplary transistor characteristics are shown.

#### 3.2. Modeling of the TTF spectra and cell-adhesion examination

To quantitatively understand the cellular adhesion mechanics, we earlier proposed a theoretical EEC model as presented in Fig. 2a (Susloparova et al., 2015). Cell-transistor coupling dynamics was detected upon various cellular stimulations, which can be monitored with the TTF-method due to cell adhesion changes (Figs. 2a, 1-4). Potential influences of the cell-cell junction can also be considered in the case when multiple cells interact with larger transistor gates, while applying an extended EEC model to account for cell-cell junctions (Hempel et al., 2021). In this work, the adhesion of single cells on UF-FETs was successfully monitored by frequency-dependent TTF-measurements with both HEK 293 and fibroblast cells. Most importantly, the sealing resistance R<sub>seal</sub> is the main parameter, which describes the adhesion strength of the cell on top of the transistor gate. This resistor is formed by the electrolyte-filled contact area between the attached part of the cell membrane and the transistor surface. In an earlier publication of our group, we derived an analytical equation R<sub>seal</sub> from experimental data of cell-transistor coupling experiments using parallel patch-clamp and transistor recordings (Wrobel et al., 2005; Pabst et al., 2007). The equation was the result from an analytical solution of the Poisson-Nernst-Planck equations in the cell-substrate

$$R_{seal} = \frac{k_B T}{4\pi e_0^2 n_{tor}^B D_{K+} h} \left[ 1 + 4 \frac{L_D^2}{r^2} \left( \frac{1}{I_0(r/L_D)} - 1 \right) \right]$$
 [1]

, where  $k_B$  is the Boltzmann constant, T is the absolute temperature,  $e_0$  is the elementary charge,  $n_{tot}^B$  is a particle density of the surrounding bath solution,  $D_{K^+}$  is the diffusion coefficient of potassium in this particular case, h is the average height of the electrolyte-filled cleft between the cellular membrane and the chip surface,  $I_0$  is the modified Bessel function, r is the cell radius, and  $L_D$  is the Debye screening length.

As described before, the TTF-spectra can also reveal the morphology of the cells, since the projected capacitive signal part for the stimulation voltage through the cell represented by  $C_{PM}$  is the serial combination of the free membrane part  $C_{FM}$  and the surface-attached membrane part in the junction  $C_{JM}$  with:

$$C_{PM} = \frac{C_{FM} \cdot C_{JM}}{C_{FM} + C_{JM}}$$
 [2]

It needs to be noted that this projected membrane capacitance  $C_{PM}$  is distinctly different from the total membrane capacitance  $C_{M}$  typically measured by patch-clamp pipettes from inside to outside of a whole cell. Due to the serial combination of the free and the attached membrane parts this projected membrane capacitance  $C_{PM}$  is generally much smaller than the typical whole-cell membrane capacitances of cells and depend on the particular cell morphology (for further explanation, please refer to the supplementary material file Fig. S4).

In the TTF-measurements with the UF-FET devices in this study, several shapes of the TTF spectra were observed, which can be described by four different time constants governing the cell-transistor contact (Equations (3)–(7)). (Schäfer et al., 2009)

$$H(i\omega) = V_{out} \cdot g_{m} \cdot \frac{(1 + i\omega\tau_{1}) \cdot (1 + i\omega\tau_{2})}{(1 + i\omega\tau_{3}) \cdot (1 + i\omega\tau_{4})}$$
[3]

$$\tau_1 = C_{PM} \cdot R_{seal} \tag{4}$$

$$\tau_2 = -\frac{C_{CL} \cdot (C_{PM} + C_{ox})}{C_{PM} \cdot g_m}$$
 [5]

$$\tau_3 = R_{seal} \cdot (C_{PM} + C_{ox}) \tag{6}$$

$$\tau_4 = 2 \cdot R_{el} \cdot C_{CL} \tag{7}$$

For a cell-free gate, the system is dominated by the time constants  $\tau_2$  and  $\tau_4$ , and their proportions. If  $\tau_4 > \tau_2$ , the TTF spectrum shows a distinct cut-off at higher frequencies, while  $\tau_2$  has little effect to the TTF spectrum within the recorded frequency band (1 Hz - 1 MHz), as shown in Fig. 2b. In special cases, when both time constants are equal, the TTF spectrum decreases after a short increase in a frequency range from 20k – 200k Hz (Fig. 2c). When  $\tau_2 \gg \tau_4$ , the normalized voltage increases dramatically for higher frequencies (>200 kHz) and the effect of  $\tau_4$  becomes invisible (Fig. 2d–e). Hence,  $\tau_4 > \tau_2$  is requested for effective cell-adhesion measurements, requiring a sufficiently high transconductance of the transistor by a given parasitic capacitance of the contact lines.

However, the influence of these four different time constants ( $\tau_1$ ,  $\tau_2$ ,  $\tau_3, \tau_4$ ) on the relevant cell-related parameters  $R_{seal}$  and  $C_{PM}$  is complex as 1) two or even three time constants need to be taken into account, 2) only  $\tau_4$  is given by the conducting line capacitance ( $C_{CL}$ ) depending on the respective chip design and the electrode and electrolyte resistance (R<sub>el</sub>). Most generally, a strong cell-transistor coverage with a large R<sub>seal</sub> value causes a large change in the TTF spectra, while the cell shape also influences the TTF spectra significantly by the projected membrane capacitance C<sub>PM</sub>. Homogenously adhered cells with a flat morphology result in higher signal changes compared to spindle shaped cells, small cells and round cells (Sommerhage et al., 2008). Generally higher seal resistances R<sub>seal</sub> are formed by flat and uniformly adherent cells (Pabst et al., 2007; Wrobel et al., 2008). A smaller cell-chip cleft height by planarized transistor gate topography with better distributed adhesion proteins at the cell-chip edge leads to the largest changes in the TTF spectra (Fromherz et al., 1991; Gleixner and Fromherz, 2006).

Under the assumption that  $C_{\text{PM}}$  is constant for roughly similarly sized cells and  $C_{PM}>C_{ox}$ , the time constants  $\tau_1$  and  $\tau_3$  fuse to one time constant. The time constant  $\tau_3$  causes a cut-off frequency at lower value in dependency on the seal resistance R<sub>seal</sub>. The observed intermediate and inclined TTF spectra are due to the interaction of  $\tau_1$  and  $\tau_3$  (Fig. 2e). In the case of  $\tau_3 > \tau_1$ , the TTF spectrum shows a saddle point or decrease in inclination before final decrease at higher frequencies that is caused by  $\tau_4$ . For increasing  $R_{seal}$ , the TTF spectrum drops at lower frequencies and  $\tau_2$  is responsible for the subsequent increase (Fig. 2e). Qualitative analysis for the four different time constants that vary with R<sub>seal</sub>, C<sub>PM</sub>, R<sub>el</sub> and gm was further done by modeling and respective values are presented in Table S2, with additional experimental cases shown in Fig. S5. In all our experiments, we utilized multiple UF-FET devices (>10 chips) and multiple biological repeats (>3). Presented results are typical examples. Generally, the low numbers of transistor channels on our chips permits a statistical analysis of the presented cell assays. However, for all measurements, the TTF results were consistent with optical microscopy controls, suggesting that the TTF method can be used as a reliable tool to monitor cell-chip coupling, electronically.

## 3.3. Cell detachment, necrosis and apoptosis examined with TTF measurements

To extract clear and quantitative information for the cell-related parameters  $R_{seal}$  and  $C_{PM}$ , trypsin, AmB and CPT-11 were applied to study the dynamics of cell-chip interaction (Fig. 3). After two days of culture, cell attachment on transistor gates was monitored by frequency-dependent TTF measurements with clear minima visible at  $\sim\!200$  kHz, compared to a cell-free reference gate (Fig. 3a–c). Notably, in experiments with conventional FET chips the cell growth and migration are significantly influenced by the topographic structures (Fig. S6). In contrast to this, the UF-FET demonstrated no influence on cell attachment and migration behavior (Fig. 3b).

Upon trypsinization, the voltage minima shifted to higher frequencies with higher transfer-function values over time, however, did not fully reach the cell-free state due to persisting cell-transistor

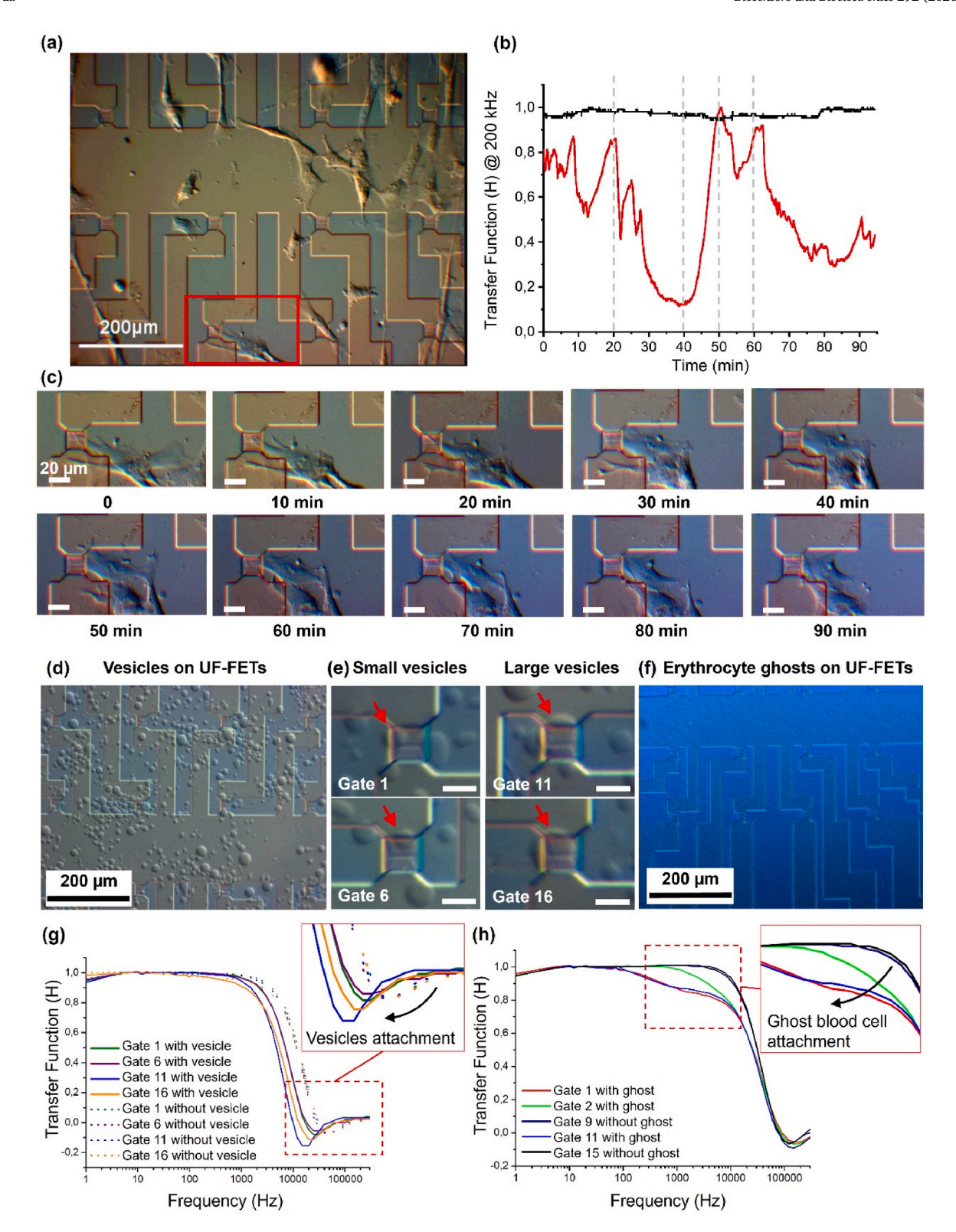


Fig. 4. Advanced applications of the TTF method using UF-FET devices (all gate sizes  $4 \times 12~\mu m^2$ ): (a–c) Subcellular fibroblast cell migration monitoring in real time with simultaneous time-dependent TTF measurements and optical tracking using an upright microscope; (d, e, g) Lipid vesicles and (f, h) erythrocyte ghost cells attached to the surface of UF-FETs chips. In both cases, the attached case could be clearly detected by a change in the TTF spectra and confirmed by optical tracking. The differences in TTF spectra from transistor gate to transistor gate can even quantify the adhesion strength and surface coverage in the individual case. Scale bars are labelled in the images (otherwise  $20~\mu m$ ).

attachment (Fig. 3d). In general, the shape of the TTF spectra did not change strongly during detachment and morphological changes, which implied that 1) the  $R_{seal}$  was significantly decreased by the trypsin activity and thereby decreasing  $\tau_3;$  2)  $C_{PM}$  did not decrease far enough to reveal the time constants  $\tau_1$  and  $\tau_3,$  3) the increase in the transfer-function value was again caused by  $\tau_2,$  which relates to the change in cellular morphology.

A time-dependent increase in the voltage amplitude of the TTF spectra at 100 kHz was also recorded upon trypsinization, where the highest change occurred in the strongly adhered cells with flat morphology (Fig. 3e–f, Fig. S7). The absolute change in the transfer function at a specific frequency could therefore contribute as an indicator for the adhesion strength of a cell. A time delay was observed in the well-attached cases eventually caused by the limited trypsin diffusion into the cell-chip clefts.

The effect of AmB on adherent cells was successfully monitored with the TTF method in both frequency and time-dependent readout modes. However, in this assay completely opposite behavior was found compared to trypsin (Fig. 3g-i). The minima were shifted to lower frequencies, along with decreased normalized voltages (~30 %), implying an increased time constant  $\tau_3$  that forced the TTF spectrum to drop during ongoing AmB action. The time constant  $\tau_1$  was not revealed, indicating that the projected capacitance C<sub>PM</sub> was not lowered, which hints to an almost unchanged morphology of the cells. The time constant  $\tau_2$  again determined the subsequent increase of the transfer function at higher frequencies. Continuous decrease was measured over time with time-dependent TTF readout after addition of AmB (Fig. 3h). Such dynamic changes suggested an enhancing Rseal upon AmB treatment, although the cell membranes could be perforated according to optical images (Fig. 3i, Fig. S8). The collapse of the cell membrane due to mechanical instability could probably form a wider coverage on the chip surface, with a larger area of the cell-chips cleft, and therefore provide higher intermediate  $R_{\text{seal}}$  values and time constants  $\tau_3.$  Despite permeability issues, we cannot completely exclude possible changes in cell adhesion in these experiments. As discussed before, both effects are combined and cannot be evaluated independently.

In a final experimental series with the HEK 293 cells, the apoptosis process of adherent cells on UF-FETs was induced by CPT-11. As a proofof-principle, simultaneous TTF measurements were conducted to monitor changes in the TTF spectra caused by the apoptosis process. The minimum frequencies of the band block effect were shifted to higher frequencies (from 100 to 200 kHz), however, the amplitude values of the transfer function remained similar (Fig. 3j). We recorded a significant increase in the transfer function values during time-dependent impedimetric measurements after CPT-11 administration, suggesting the loss of cell adhesion during apoptosis (Fig. 3k). As described in the material and methods section, the ISFET devices can be read out either in potentiometric or in impedimetric mode. We speculated that eventually during membrane perforation, local pH changes could occur at the gate leading to changes in the potentiometric signal. Such signals should be evident in the low frequency regime of the TTF spectrum. However, the quasipotentiometric measurements at 1 Hz showed no difference over an extended recording period of almost 2 h (Fig. S9). It should be noted that by applying proper readout electronics and frequency filtering, the ISFET devices could reveal potentiometric and impedimetric changes at the transistor gate in parallel. To proof that indeed an apoptosis cascade was triggered in the cells, we utilized fluorescence microscopy after staining with annexin-V and propidium iodide, in order to distinguish an early from a late apoptosis status, respectively (Fig. 3l, Fig. S10).

#### 3.4. Single cell migration monitored with UF-FETs

Different from cellular adhesion, the migration behavior of cells can be divided in processes at the cell front, underneath the cell body, and at the cell rear. In our experiments, we monitored cellular migration with time-dependent TTF measurements. In parallel, we recorded microscopy images with the upright microscope and related these to the electronic recordings. Due to the high signal-to-noise-ratio of the TTF method and the ultra-flat surfaces and the small size of the transistor gates of the UF-FETs, even subcellular processes like filopodia or lamellipodia expansion and retraction were successfully recorded. We describe in the following a typical measurement of a fibroblast cell migration on the gate of an UF-FET (Fig. 4a–c).

The highly unsteady change in the transfer function amplitude at 200 kHz was observed for dynamic cell membrane movement over the gate, compared to a cell-free gate as a control (Fig. 4b). The fibroblasts activity at the cell front was recorded when approaching and reacting from the gate (0-20 min). Only small signal changes were caused by filopodia and lamellipodia movements with similar duration, indicating their minor size and adhesive strength. Even these tiny effects could be tracked by out method using the UF-FETs. When the fibroblasts were stabilizing and completely covering the transistor gate, a significant decrease in the transfer function amplitude was observed (20-40 min). As a result of the dynamic cell migration, a subsequent increase to a cellfree level was observed when the cell body was leaving the gate (40-60 min). When the cell migrated back onto the gate afterwards, a continuous decrease in normalized voltage was again observed along with cellgate coverage, gradually stabilizing after 90 min. The whole migration process at different time points was visible and in line with optical microscope images (Fig. 4b-c), providing reliable evidence for real-time subcellular monitoring of the cellular dynamic during migration.

#### 3.5. Vesicles and erythrocyte ghosts' attachment on FETs

We further utilized the TTF readout method with UF-FETs to record the cell-substrate adhesion of lipid vesicles and erythrocyte ghost cells (Fig. 4d–h). In vesicle attachment experiments (Fig. 4d, e, g), due to the low conductivity of the glucose buffer large time constants  $\tau_4$  were observed with a significant drop in the transfer function amplitudes at low frequencies.

The minima of the TTF spectra shifted to lower frequencies with lower transfer function values during attachment, indicating the influence of  $\tau_3$ , which corresponds to a strong cell adhesion state. From the theory, we should be able to detect different  $C_{PM}$  values between smaller and larger vesicles. However, in our experiments the differences could not be detected in the time constant  $\tau_1$ . A reason could be the too large value for the time constant  $\tau_4$  caused by the large electrolyte resistance  $R_{el}$  of the glucose buffer. To reveal larger differences in the TTF spectra for these measurements, we would need to design chips with much smaller contact line capacitances  $C_{CL}$  to suppress the influence of the time constant  $\tau_4$ .

Similar constellation was found in the adhesion measurements using erythrocyte ghosts (Fig. 4f–h). Due to the larger conductivity of the ISP buffer much higher than the one of the glucose buffer, the TTF spectra exhibited an intermediated saddle shape. Hence,  $\tau_4$  affected the TTF spectrum at higher frequencies and revealed influences of the time constant  $\tau_1.$  All four different time constants were visible in these TTF spectra, with the following relation:  $\tau_2 < \tau_4 < \tau_1 < \tau_3.$  However, small changes in the different parameters influencing these time constants could lead to a suppression of a single time constant - particularly in very sensitive measurements such as the adhesion of the tiny erythrocyte ghosts. Therefore, the TTF method and the design of the UF-FETs need to be carefully tuned for optimized assays of either one of the above applications presented here.

#### 4. Conclusion

In this work, the method of transistor-transfer function measurements was successfully applied to qualitatively characterize the contact between cells and ultra-flat FETs, as well as other artificial and cellular membrane-based systems attached to the transistor surfaces. Both frequency- and time-dependent measurements were conducted to reveal

various properties of the TTF method in combination with the designed UF-FET devices. Multiple shapes of the TTF spectra were identified and interpreted concerning four different time constants of the spectra. These time constants are critically dependent on passive, chip-related factors such FET transconductance, transistor gate capacitance and the corresponding contact line capacitance at source and drain contacts. The resistance of the electrolyte solution utilized during measurements plays a significant role as well. Once these parameters are optimized, TTF measurements can reveal cell-related parameters such as the sealing resistance between the cell membrane and the transistor surface, which relates to the adhesion strength, and the projected membrane capacitance, which reveals the morphology of the individual cell. However, both effects are not completely de-coupled in the time constants. When larger transistors are utilized, the influence of cell-cell contacts can be seen as well just like in standard ECIS measurements using larger metal electrodes.

From our measurements using the UF-FET devices developed in this work, the adhesive strength of HEK 293 cells was qualitatively determined and found to correlate with cell morphology. The dynamics of cell detachment and changes in membrane permeability were monitored following stimulation with trypsin and AmB, respectively. All measurements at the single-cell level were highly consistent with parallel microscopy controls. Drawback was, however, that we had no procedure to align cells onto the transistor gates for the analysis. Cells were arbitrarily seeded and only those attached to the transistor gates of the chip could be analyzed. Nevertheless, a fluorescence staining method was introduced to detect cell apoptosis, with simultaneous impedimetric and potentiometric changes of the transistor signals in normalized voltages observed following CPT-11 treatment. For such pharmacological assays, however, the current chip design of the UF-FETs is not suitable, since they only offer 16 transistor channels. For a statistical evaluation of the drug effects of colonies of cells, many more transistors would be needed for a meaningful statistical analysis.

In our current experimental design, quantitative biological or pharmacological assays on single cells are not possible. For such aim we would need to chemically address a small area on chip with a precise dosing of a chemical or drug, which would need a sophisticated microfluidic addressing concept. Therefore, in contrast to the classical patch-clamp technique with single cell perfusion, we cannot provide pharmacokinetics data in single cell studies. Nevertheless, the concept of utilizing ultra-flat field-effect transistors for impedance sensing complements the classical ECIS method with a single cell resolution for adhesion monitoring leaving room for many complementary applications.

Compared to an earlier publication of our group with quasi-planar field-effect transistors, the UF-FETs realized in this work have also flat topography with less than 30 nm high features in their gate areas, where the actual adhesion detection takes place. This property enabled cell-substrate adhesion monitoring in so far not reachable sub-cellular resolution. In the single-cell experiments presented in this work, fibroblast cell migration was monitored time-dependently at the sub-cellular level using the TTF spectra analysis, revealing sub-cellular adhesion patterns of individual filopodia and groups of lamellipodia. Different adhesion behaviors were observed at the cell front, cell body, and cell rear. However, significant values for  $R_{\rm seal}$  and  $C_{\rm PM}$  could not be determined from the experimental results due to the complexity of the interactions within system. A file of a time lapse video is provided in the supplementary material, which shows the sub-cellular resolution of the single-cell experiment.

In additional proof-of-concept experiments, lipid membrane vesicles and erythrocyte ghosts were successfully prepared and their attachment to the gates of UF-FET devices was detected. The resulting TTF spectra were analyzed concerning the corresponding time constants, providing strong experimental evidence supporting membrane-transistor interaction models.

This work has effectively demonstrated that the TTF method using

ultra-flat FET devices can dynamically monitor cell and lipid membrane adhesion to the oxide surfaces of the transistor gates. However, future experiments should focus on advancing the analytical approaches and deepening our understanding of the interplay of the involved time constants. A definite reference system would be necessary to calibrate the system and to determine the exact cell-related values for membrane adhesion. The TTF method with FET devices described in this work, however, offers very promising future potential as complementary method to the classical ECIS assays. With our devices it is possible to electronically monitor the cell-substrate adhesion for different cell biological questions over extended periods with so far unmatched spatial resolution.

#### CRediT authorship contribution statement

Ziyu Gao: Writing – review & editing, Writing – original draft, Data curation. Susanne Schäfer: Visualization, Validation, Investigation, Formal analysis, Data curation. Regina Stockmann: Methodology, Investigation, Data curation. Bernd Hoffmann: Validation, Supervision, Investigation. Rudolf Merkel: Supervision, Funding acquisition, Conceptualization. Andreas Offenhäusser: Supervision, Methodology, Funding acquisition, Conceptualization. Sven Ingebrandt: Writing – review & editing, Writing – original draft, Visualization, Validation, Supervision, Methodology, Investigation, Funding acquisition, Formal analysis, Conceptualization.

#### **Ethical statement**

Fibroblasts were isolated from the umbilical cord of 19-day-old Wistar rat embryos. In brief,  $CO_2$  anesthetized pregnant rats were decapitated, the embryos were removed and umbilical cords were prepared under sterile conditions. Other parts of the rat embryos were used for parallel experiments of our colleagues. Cell culture was conducted in accordance with national guidelines for the care and maintenance of laboratory animals and approved by the Landesumweltamt für Natur, Umwelt und Verbraucherschutz Nordrhein-Westfalen, Recklinghausen, Germany, in accordance with  $\S 6$  TierschG.,  $\S 4$  TSchG i.V. and  $\S 2$  TierSchVerV.

For the experiments with the human erythrocyte ghost cells, 25 mL of fresh blood was donated by the second author of this manuscript (S. Schäfer). It was taken with a standard procedure by experienced staff at the Medical Service Facility of the Forschungszentrum Jülich GmbH. This was done voluntarily and the researcher provided a written consent of her voluntary participation in this study.

#### **Declaration of competing interest**

The authors declare that they have no known competing financial interests or personal relationships that could have appeared to influence the work reported in this paper.

#### Acknowledgements

Funding by the Forschungszentrum Jülich GmbH is greatly acknowledged. The authors thank Rita Fricke (née Helpenstein) for her support with the cell culture.

#### Appendix A. Supplementary data

Supplementary data to this article can be found online at https://doi. org/10.1016/j.bios.2025.118087.

#### Data availability

Data will be made available on request.

#### References

- Abagnale, G., Steger, M., Nguyen, V.H., Hersch, N., Sechi, A., Joussen, S., Denecke, B., Merkel, R., Hoffmann, B., Dreser, A., Schnakenberg, U., Gillner, A., Wagner, W., 2015. Surface topography enhances differentiation of mesenchymal stem cells towards osteogenic and adipogenic lineages. Biomaterials 61, 316–326.
- Angelova, M.I., Dimitrov, D.S., 1986. Liposome electroformation. Faraday Discuss 81, 303–311.
- Angelova, M.I., Dimitrov, D.S., 1987. Swelling of charged lipids and formation of liposomes on electrode surfaces. Mol. Cryst. Liq. Cryst. 152, 89–104.
- Atanasov, V., Knorr, N., Duran, R.S., Ingebrandt, S., Offenhausser, A., Knoll, W., Koper, I., 2005. Membrane on a chip: a functional tethered lipid bilayer membrane on silicon oxide surfaces. Biophys. J. 89 (3), 1780–1788.
- Bihr, T., Fenz, S., Sackmann, E., Merkel, R., Seifert, U., Sengupta, K., Smith, A.S., 2014. Association rates of membrane-coupled cell adhesion molecules. Biophys. J. 107 (11), L33–L36.
- Blaschke, S.J., Demir, S., Konig, A., Abraham, J.A., Vay, S.U., Rabenstein, M., Olschewski, D.N., Hoffmann, C., Hoffmann, M., Hersch, N., Merkel, R., Hoffmann, B., Schroeter, M., Fink, G.R., Rueger, M.A., 2020. Substrate elasticity exerts functional effects on primary microglia. Front. Cell. Neurosci. 14, 590500.
- Braun, D., Fromherz, P., 2004. Imaging neuronal seal resistance on silicon chip using fluorescent voltage-sensitive dye. Biophys. J. 87 (2), 1351–1359.
- Cheng, J.T., Witty, R.T., Robinson, R.R., Yarger, W.E., 1982. Amphotericin-B nephrotoxicity - increased renal resistance and tubule permeability. Kidney Int. 22 (6), 626–633.
- Conti, J.A., Kemeny, N.E., Saltz, L.B., Huang, Y., Tong, W.P., Chou, T.C., Sun, M., Pulliam, S., Gonzalez, C., 1996. Irinotecan is an active agent in untreated patients with metastatic colorectal cancer. J. Clin. Oncol. 14 (3), 709–715.
- de Moraes, A., Kubota, L., 2016. Recent trends in field-effect transistors-based immunosensors. Chemosensors 4 (4), 1–20.
- Dimitrov, D.S., Angelova, M.I., 1988. Lipid swelling and liposome formation mediated by electric-fields. Bioelectrochem. Bioenerg. 19 (2), 323–336.
- Estes, D.J., Mayer, M., 2005. Electroformation of giant liposomes from spin-coated films of lipids. Colloids Surf. B Biointerfaces 42 (2), 115–123.
- França, F.D., Ferreira, A.F., Lara, R.C., Rossoni, J.V., Costa, D.C., Moraes, K.C.M.,
   Tagliati, C.A., Chaves, M.M., 2014. Alteration in cellular viability, pro-inflammatory cytokines and nitric oxide production in nephrotoxicity generation by amphotericin
   B: involvement of PKA pathway signaling. J. Appl. Toxicol. 34 (12), 1285–1292.
- Fromherz, P., Kiessling, V., Kottig, K., Zeck, G., 1999. Membrane transistor with giant lipid vesicle touching a silicon chip. Appl. Phys. A Mater. Sci. Process. 69 (5), 571–576.
- Fromherz, P., Offenhausser, A., Vetter, T., Weis, J., 1991. A neuron-silicon junction a retzius cell of the leech on an insulated-gate field-effect transistor. Science 252 (5010), 1290–1293.
- GhoshMoulick, R., Vu, X.T., Gilles, S., Mayer, D., Offenhäusser, A., Ingebrandt, S., 2009. Impedimetric detection of covalently attached biomolecules on field-effect transistors. Phys. Status Solidi A-Appl. Mat. 206 (3), 417–425.
- Giaever, I., Keese, C.R., 1984. Monitoring fibroblast behavior in tissue-culture with an applied electic-field. Proc. Natl. Acad. Sci. U. S. A. 81 (12), 3761–3764.
- Giaever, I., Keese, C.R., 1991. Micromotion of mammalian-cells measured electrically. Proc. Natl. Acad. Sci. U. S. A. 88 (17), 7896–7900.
- Giaever, I., Keese, C.R., 1993. A morphological biosensor for mammalian-cells. Nature 366 (6455), 591–592.
- Gleixner, R., Fromherz, P., 2006. The extracellular electrical resistivity in cell adhesion. Biophys. J. 90 (7), 2600–2611.
- Han, Y., Offenhäusser, A., Ingebrandt, S., 2006. Detection of DNA hybridization by a field-effect transistor with covalently attached catcher molecules. Surf. Interface Anal. 38 (4), 176–181.
- Hempel, F., Law, J.K.Y., Ingebrandt, S., 2019. Transistor-based impedimetric monitoring of single cells. In: Wegener, J. (Ed.), Label-Free Monitoring of Cells in Vitro. Springer International Publishing, Cham, pp. 77–110.
- Hempel, F., Law, J.K.Y., Nguyen, T.C., Lanche, R., Susloparova, A., Vu, X.T., Ingebrandt, S., 2021. PEDOT:PSS organic electrochemical transistors for electrical cell-substrate impedance sensing Down to single cells. Biosens. Bioelectron. 180, 1–7
- Hempel, F., Nguyen, T.C., Law, J.K.Y., Ingebrandt, S., 2015. The influence of medium conductivity on ECIS measurements with field-effect transistor arrays. Phys. Status Solidi A-Appl. Mat. 212 (6), 1260–1265.
- Hou, Y., Xie, W., Yu, L., Camacho, L.C., Nie, C., Zhang, M., Haag, R., Wei, Q., 2020. Surface roughness gradients reveal topography-specific mechanosensitive responses in human mesenchymal stem cells. Small 16 (10), e1905422.
- Humphrey, J.D., Dufresne, E.R., Schwartz, M.A., 2014. Mechanotransduction and extracellular matrix homeostasis. Nat. Rev. Mol. Cell Biol. 15 (12), 802–812.
- Hurst, S., Vos, B.E., Brandt, M., Betz, T., 2021. Intracellular softening and increased viscoelastic fluidity during division. Nat. Phys. 17 (11), 1270–1276.
- Ingebrandt, S., Han, Y., Nakamura, F., Poghossian, A., Schöning, M.J., Offenhäusser, A., 2007. Label-free detection of single nucleotide polymorphisms utilizing the differential transfer function of field-effect transistors. Biosens. Bioelectron. 22 (12), 2834–2840
- Koppenhöfer, D., Susloparova, A., Doctor, D., Stauber, R.H., Ingebrandt, S., 2013. Monitoring nanoparticle in-duced cell death in H441 cells using field-effect transistors. Biosens. Bioelectron. 40, 89–95.
- Koppenhöfer, D., Kettenbaum, F., Susloparova, A., Law, J.K.Y., Vu, X.T., Schwab, T., Schäfer, K.H., Ingebrandt, S., 2015a. Neurodegeneration through oxidative stress: monitoring hydrogen peroxide induced apoptosis in primary cells from the

- subventricular zone of BALB/c mice using field-effect transistors. Biosens. Bioelectron. 67, 490–496.
- Koppenhöfer, D., Susloparova, A., Law, J.K.Y., Vu, X.T., Ingebrandt, S., 2015b. Electronic monitoring of single cell-substrate adhesion events with quasi-planar field-effect transistors. Sens. Actuator B-Chem. 210, 776–783.
- Lauer, L., Ingebrandt, S., Scholl, M., Offenhäusser, A., 2001. Aligned microcontact printing of biomolecules on microelectronic device surfaces. IEEE (Inst. Electr. Electron. Eng.) Trans. Biomed. Eng. 48 (7), 838–842.
- Law, J.K.Y., Susloparova, A., Vu, X.T., Zhou, X., Hempel, F., Qu, B., Hoth, M., Ingebrandt, S., 2015. Human T cells monitored by impedance spectrometry using field-effect transistor arrays: a novel tool for single-cell adhesion and migration studies. Biosens. Bioelectron. 67, 170–176.
- Leung, C.M., de Haan, P., Ronaldson-Bouchard, K., Kim, G.-A., Ko, J., Rho, H.S., Chen, Z., Habibovic, P., Jeon, N.L., Takayama, S., Shuler, M.L., Vunjak-Novakovic, G., Frey, O., Verpoorte, E., Toh, Y.-C., 2022. A guide to the organ-on-a-chip. Nat. Rev. Methods Primers 2 (1), 1–29.
- Lisin, R., Ginzburg, B.Z., Schlesinger, M., Feldman, Y., 1996. Time domain dielectric spectroscopy study of human cells .1. erythrocytes and ghosts. Biochim. Biophys. Acta-Biomembr. 1280 (1), 34–40.
- Miller, L.F., 2000. Controlled collapse reflow chip joining. IBM J. Res. Dev. 44 (1.2),
- Morgan, H., Sun, T., Holmes, D., Gawad, S., Green, N.G., 2007. Single cell dielectric spectroscopy. J. Phys. D Appl. Phys. 40 (1), 61–70.
- Offenhausser, A., Sprossler, C., Matsuzawa, M., Knoll, W., 1997. Field-effect transistor array for monitoring electrical activity from mammalian neurons in culture. Biosens. Bioelectron. 12 (8), 819–826.
- Pabst, M., Wrobel, G., Ingebrandt, S., Sommerhage, F., Offenhäusser, A., 2007. Solution of the poisson-nernst-planck equations in the cell-substrate interface. Eur. Phys. J. E 24 (1), 1–8.
- Pradhan, R., Mitra, A., Das, S., 2012. Characterization of electrode/electrolyte interface of ECIS devices. Electroanalysis 24 (12), 2405–2414.
- Price, D.T., Rahman, A.R.A., Bhansali, S., 2009. Design rule for optimization of microelectrodes used in electric cell-substrate impedance sensing (ECIS). Biosens. Bioelectron. 24 (7), 2071–2076.
- Rahman, A.R.A., Price, D.T., Bhansali, S., 2007. Effect of electrode geometry on the impedance evaluation of tissue and cell culture. Sens. Actuator B-Chem. 127 (1), 89–96.
- Schäfer, S., Eick, S., Hofmann, B., Dufaux, T., Stockmann, R., Wrobel, G., Offenhäusser, A., Ingebrandt, S., 2009. Time-dependent observation of individual cellular binding events to field-effect transistors. Biosens. Bioelectron. 24 (5), 1201–1208.
- Schoning, M.J., Poghossian, A., 2002. Recent advances in biologically sensitive field-effect transistors (BioFETs). Analyst 127 (9), 1137–1151.
- Shoute, L.C.T., Abdelrasoul, G.N., Ma, Y.H., Duarte, P.A., Edwards, C., Zhuo, R., Zeng, J., Feng, Y.W., Charlton, C.L., Kanji, J.N., Babiuk, S., Chen, J., 2023. Label-free impedimetric immunosensor for point-of-care detection of COVID-19 antibodies. Microsyst. Nanoeng. 9 (3), 1–16.
- Solowiej-Wedderburn, J., Dunlop, C.M., 2022. Sticking around: cell adhesion patterning for energy minimization and substrate mechanosensing. Biophys. J. 121 (9), 1777–1786.
- Sommerhage, F., Helpenstein, R., Rauf, A., Wrobel, G., Offenhäusser, A., Ingebrandt, S., 2008. Membrane allocation profiling: a method to characterize three-dimensional cell shape and attachment based on surface reconstruction. Biomaterials 29 (29), 3927–3935.
- Steck, T.L., Kant, J.A., 1974. Preparation of impermeable ghosts and inside-out vesicles from human erythrocyte membranes. Methods Enzymol. 172–180. Academic Press.
- Stolwijk, J.A., Wegener, J., 2019. Impedance-based assays along the life span of adherent mammalian cells in vitro: from initial adhesion to cell death. In: Wegener, J. (Ed.), Label-Free Monitoring of Cells in Vitro. Springer International Publishing, Cham, pp. 1–75.
- Susloparova, A., Koppenhöfer, D., Law, J.K.Y., Vu, X.T., Ingebrandt, S., 2015. Electrical cell-substrate impedance sensing with field-effect transistors is able to unravel cellular adhesion and detachment processes on a single cell level. Lab Chip 15 (3), 668–679.
- Susloparova, A., Koppenhöfer, D., Vu, X.T., Weil, M., Ingebrandt, S., 2013. Impedance spectroscopy with field-effect transistor arrays for the analysis of anti-cancer drug action on individual cells. Biosens. Bioelectron. 40 (1), 50–56.
- Susloparova, A., Vu, X.T., Koppenhöfer, D., Law, J.K.Y., Ingebrandt, S., 2014. Investigation of ISFET device parameters to optimize for impedimetric sensing of cellular adhesion. Phys. Status Solidi A-Appl. Mat. 211 (6), 1395–1403.
- Sze, S.M., 2012. Semiconductor Devices: Physics and Technology. John Wiley & Sons, Singapore Pte. Limited.
- Uslu, F., Ingebrandt, S., Mayer, D., Böcker-Meffert, S., Odenthal, M., Offenhäusser, A., 2004. Labelfree fully electronic nucleic acid detection system based on a field-effect transistor device. Biosens. Bioelectron. 19 (12), 1723–1731.
- Varlam, D.E., Siddiq, M.M., Parton, L.A., Rüssmann, H., 2001. Apoptosis contributes to amphotericin B-induced nephrotoxicity. Antimicrob. Agents Chemother. 45 (3), 679–685.
- Vora, K., Kordas, N., Seidl, K., 2023. Label-free, impedance-based biosensor for kidney disease biomarker uromodulin. Sensors (Basel) 23 (24), 1–9, 9696.
- Wall, M.E., Wani, M.C., Cook, C.E., Palmer, K.H., McPhail, A.T., Sim, G.A., 1966. Plant antitumor agents. I. The isolation and structure of camptothecin, a novel alkaloidal leukemia and tumor inhibitor from camptotheca acuminata1,2. J. Am. Chem. Soc. 88 (16), 3888–3890.

- Wrobel, G., Seifert, R., Ingebrandt, S., Enderlein, J., Ecken, H., Baumann, A., Kaupp, U. B., Offenhäusser, A., 2005. Cell-transistor coupling: investigation of potassium currents recorded with p- and n-Channel FETs. Biophys. J. 89 (5), 3628–3638.
- Wrobel, G., Höller, M., Ingebrandt, S., Dieluweit, S., Sommerhage, F., Bochem, H.P., Offenhäusser, A., 2008. Transmission electron microscopy study of the cell-sensor interface. J. R. Soc. Interface 5 (19), 213–222.
- Wu, D., Shi, W.G., Zhao, J., Wei, Z.R., Chen, Z.J., Zhao, D.W., Lan, S.J., Tai, J.D., Zhong, B.H., Yu, H., 2016. Assessment of the chemotherapeutic potential of a new camptothecin derivative, ZBH-1205. Arch. Biochem. Biophys. 604, 74–85.
- Zeck, G., Fromherz, P., 2003. Repulsion and attraction by extracellular matrix protein in cell adhesion studied with nerve cells and lipid vesicles on silicon chips. Langmuir 19 (5), 1580–1585.
- Zhu, G.Y., Zhang, Y., Xu, H.X., Jiang, C., 1998. Identification of endogenous outward currents in the human embryonic kidney (HEK 293) cell line. J. Neurosci. Methods 81 (1–2), 73–83.